

Universality in Efimov associated tetramers in ^4He

E. Hiyama*

RIKEN Nishina Center, RIKEN, Wako 351-0198, Japan

M. Kamimura†

Department of Physics, Kyushu University, Fukuoka 812-8581, Japan,
RIKEN Nishina Center, RIKEN, Wako 351-0198, Japan

(Dated: January 21, 2020)

We calculated, using seven *realistic* ^4He - ^4He potentials in the literature, the Efimov spectra of ^4He trimer and tetramer and analyzed the universality of the systems. The three-(four-)body Schrödinger equations were solved fully nonadiabatically with the high-precision calculation method employed in our previous work on the ^4He trimer and tetramer [Phys. Rev. A **85**, 022502 (2012); **85**, 062505 (2012)]. We found the following universality in the four-boson system: i) The critical scattering lengths at which the tetramer ground and excited states couple to the four-body threshold are independent of the choice of the two-body realistic potentials in spite of the difference in the short-range details and do not contradict the corresponding values observed in the experiments in ultracold alkali atoms when scaled with the van der Waals length r_{vdW} , and ii) the four-body hyperradial potential has a repulsive barrier at the four-body hyperradius $R_4 \approx 3 r_{\text{vdW}}$, which prevents the four particles from getting close together to explore nonuniversal features of the interactions at short distances. This result is an extension of the universality in Efimov trimers that the appearance of the repulsive barrier at the three-body hyperradius $R_3 \approx 2 r_{\text{vdW}}$ makes the critical scattering lengths independent of the short-range details of the interactions as reported in the literature and also in the present work for the ^4He trimer with the realistic potentials.

I. INTRODUCTION

The universal physics of few particles interacting with resonant short-range interactions, commonly referred to as Efimov physics [1], has intensively studied in recent years both experimentally and theoretically (e.g. [2–4] for a review). The resonant short-range two-body interaction with the s -wave scattering length a at the unitary limit $a \rightarrow \pm\infty$ generates the effective three-body attraction that supports an infinite number of weakly bound three-body states, known as the Efimov trimers, with the peculiar geometric universal scaling of their energies. For a potential with a finite scattering length a , only a finite number of the three-body bound states exist. The critical scattering length, $a_-^{(0)}$, for the appearance of the first Efimov state at the three-body threshold on the $a < 0$ side, often referred to as the three-body parameter, was initially considered as a nonuniversal quantity to be affected by the short-range details of the interactions. The absolute position of $a_-^{(0)}$, which determines the overall scale of the whole Efimov spectrum, is not predicted by the low-energy effective theories [1, 3, 4].

However, several recent experiments with identical ultracold alkali atoms suggested that the three-body parameter $a_-^{(0)}$ might be universal since the observed values in Refs. [5–16] are approximately the same in units of the van der Waals length r_{vdW} for different atoms, $a_-^{(0)}/r_{\text{vdW}} \approx -9.5 \pm 15\%$ as summarized in Refs. [12, 17–19], where $r_{\text{vdW}} = \frac{1}{2}(mC_6/\hbar^2)^{1/4}$ with the atomic mass m and the coefficient C_6 of the long-range potential r^{-6} [20].

This interesting result has stimulated the theoretical studies in Refs. [18, 21–27]. In Ref. [18], with a numerical study in the adiabatic hyperspherical representation, the universality of the three-body parameter $a_-^{(0)}/r_{\text{vdW}}$ has been understood as follows: The origin of the universality is related to the suppression of the probability to find two particles at distances $r \lesssim r_{\text{vdW}}$ where the pairwise interaction features a deep well supporting many two-body bound states or a short-range hard-core repulsion. This suppression leads to the formation of the universal three-body potential barrier around the three-body hyperradius $R_3 \approx 2 r_{\text{vdW}}$ (see Eq. (2.2) below for the definition of the A -body hyperradius). This barrier prevents the three particles from simultaneously getting close together to explore nonuniversal features of the interactions at short distances. Reference [26] elaborated on this physical mechanism by elucidating how the two-body suppression leads to appearance of the universal barrier at $R_3 \approx 2 r_{\text{vdW}}$.

As for the ^4He trimer interacting with a realistic ^4He potential that has a strong repulsive core at $r \approx r_{\text{vdW}}$ and supports only one two-body bound state, one of the present authors (E.H.) and the collaborators [24] showed, by performing a nonadiabatic three-body calculation, $a_-^{(0)}$ is consistent with the observed value of the three-body parameter in alkali atoms when scaled with the effective range.

One of the aims of the present paper is, using the same framework, the Gaussian expansion method (GEM) [28–32] for few-body systems, as in our previous papers [33] and [34] (hereafter referred to as paper I and paper II, respectively), to calculate the Efimov spectra of the ^4He trimer with the seven different realistic ^4He potentials [35–45]. We show that the calculated three-body parameters $a_-^{(v)}$ for the ground ($v = 0$) and excited ($v = 1$) states are independent of the difference in the short-range details of the realistic potentials and are consistent with the observed values of the first and second Efi-

*Electronic address: hiyama@riken.jp

†Electronic address: mkamimura@riken.jp

mov resonances in the experiments for the alkali trimers when scaled with the van der Waals length.

From the ^4He trimer wave functions described with the three sets of the Jacobi coordinates, we derive the three-body potential $U_3(R_3)$ as a function of the three-body hyperradius R_3 and show that $U_3(R_3)$ has a repulsive core at $R_3 \approx 2 r_{\text{vdW}}$ and the three-body probability density inside the core is heavily suppressed both in the ground and excited states. This supports, from the view point of the realistic interactions, the finding [18, 26] of the appearance of the three-body repulsion universally at $R_3 \approx 2 r_{\text{vdW}}$ in the first Efimov trimer state.

As long as the tetramers of the alkali atoms are concerned, recent experiments have observed the scattering lengths $a_-^{(4,0)}$ and $a_-^{(4,1)}$, at which the first and second universal four-body states tied to the first Efimov trimer state emerges at the four-body threshold on the $a < 0$ side. The data [2, 7, 14, 15] exhibit a universal property $a_-^{(4,0)}/r_{\text{vdW}} \approx -(3 - 4.5)$ and $a_-^{(4,1)}/r_{\text{vdW}} \approx -(7 - 8.5)$.

Another aim of this paper is to calculate the four-body Efimov spectra of the ^4He tetramer states ($v = 0, 1$) associated with the trimer ground state using the same realistic ^4He potentials as above and present that the calculated values of the $a_-^{(4,0)}$ and $a_-^{(4,1)}$ are independent of the details of the potentials at short inter-particle separations and do not contradict the observed values when scaled with the van der Waals length. From the calculated tetramer wave function described with the full 18 sets of the Jacobi coordinates, we derive a four-body potential $U_4(R_4)$ as a function of the four-body hyperradius R_4 and show that the repulsive core is located at $R_4 \approx 3 r_{\text{vdW}}$ and the four-body probability density inside the core is heavily suppressed both in the ground and excited states.

The region suppressed by the three-(four-)body barrier in the ^4He trimer (tetramer) is significantly larger than the region that is trivially excluded by the two-body repulsive core at $r \approx r_{\text{vdW}}$, which makes the critical scattering lengths insensitive to the short-range physics.

It is to be noted that the present work has the following limitation: The realistic ^4He - ^4He potential with the van der Waals tail is a single-channel potential into which excitation of the interacting particles is renormalized, and no excited channel is explicitly incorporated in the present framework. Therefore, we shall compare our results with the property of the broad Feshbach resonances in the ultracold alkali atoms and consider that our single-channel model is not applicable to the narrow resonances generated by the multi-channel effects (cf. for instance, Refs. [20, 46]).

This paper is organized as follows: In Sec. II, we briefly explain the method and realistic ^4He potentials. In Sec. III, we calculate the Efimov spectrum of the ^4He trimer and derive the three-body parameters $a_-^{(v)}$ ($v = 0, 1$) which are compared with the corresponding observed values. The three-body hyperradial potentials $U_3^{(v)}(R_3)$ is derived. In Sec. IV, we calculate the Efimov spectrum of the ^4He tetramer and derive the critical scattering lengths $a_-^{(4,v)}$ ($v = 0, 1$) which are compared with the observed values. The four-body hyperradial potential $U_4^{(v)}(R_4)$ is derived. Summary is given in Sec. V.

II. METHOD AND INTERACTIONS

Soon after the Efimov effect was predicted in the early 1970s, the ^4He trimer was expected to have bound states of Efimov type since the ^4He - ^4He interaction gives a large scattering length $a \sim 115 \text{ \AA}$ (much greater than the potential range $\sim 10 \text{ \AA}$) and a very small ^4He dimer binding energy $B_2 \sim 1 \text{ mK}$ with the large mean radius $\langle r \rangle \sim 54 \text{ \AA}$. This fact strongly stimulated a large number of three-body calculations of ^4He atoms, which predicted existence of the ground state and a very weakly bound excited states (references in papers I and II as well as the latest result for the ^4He dimer, trimer and tetramer using realistic ^4He potentials).

Experimentally, Ref. [47] obtained $\langle r \rangle = 52 \pm 4 \text{ \AA}$ and estimated $a = 104_{-18}^{+8} \text{ \AA}$ and $B_2 = 1.1_{-0.2}^{+0.3} \text{ mK}$ using a crude model of $a = 2\langle r \rangle$ and $B_2 = \hbar^2/4m\langle r \rangle^2$; a more appropriate estimation was recently given in Ref. [45] as $a = 100.2_{-7.9}^{+8.0} \text{ \AA}$ and $B_2 = 1.30_{-0.19}^{+0.25} \text{ mK}$. The ^4He trimer ground state has been observed in Ref. [48] to have the ^4He - ^4He bond length of 11_{-5}^{+4} \AA in agreement with theoretical predictions, whereas a reliable experimental evidence for the ^4He trimer excited state is still missing.

Although the Efimov trimers have been observed in experiments with ultracold alkali atoms, the study of ^4He clusters has been providing with the fundamental information to the universal Efimov physics. In this paper, we intend to add the new understanding that even ^4He potentials are consistent with measurements in ultracold atoms for broad Feshbach resonances of trimers and tetramers tied to the trimer ground states and that this fact shows the large extent of universality in three- and four-body systems with interactions featuring van der Waals tails.

A. Gaussian expansion method for few body systems

In order to solve accurately the three- and four-body Schrödinger equations for the ^4He trimer and tetramer, we use the Gaussian expansion method for few-body systems [28–32] explained precisely in papers I and II. We employ the seven kinds of realistic ^4He - ^4He potentials; names of the potentials are LM2M2 [35], TTY [36], HFD-B [37], HFD-B3-FCI1 [38–40], SAPT96 [40–42], CCSAPT07 [43], and PCKLJS [44, 45]. Among them the PCKLJS is currently the most sophisticated and accurate as explained in paper II, while the LM2M2 has most popularly been used in the literature.

The realistic ^4He potentials has a strong repulsive core (Fig. 1), which makes it technically challenging to solve the low-energy few-body problems accurately. As was shown in papers I and II, however, our method is suitable for describing both the short-range correlations (without *a priori* assumption of any two-body correlation function) and the long-range asymptotic behavior of the ^4He trimer and tetramer.

The wave function of the A -body ^4He -atom system ($A = 2 - 4$), say Ψ_A , is obtained by solving the Schrödinger equa-

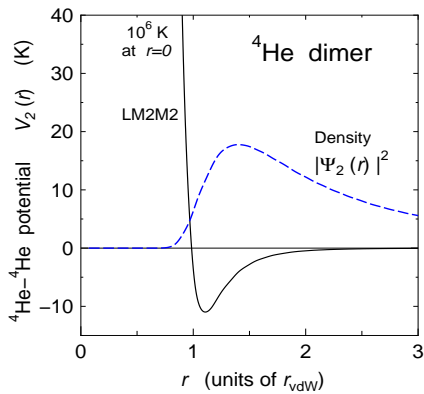


FIG. 1: (Color online) The LM2M2 potential $V_2(r)$, one of the realistic ${}^4\text{He}$ potentials, is shown as the black solid curve. The dashed blue curve shows the density of the dimer $|\Psi_2(r)|^2$ (in arbitrary unit) at $E_2 = -1.309$ mK, so weakly bound compared with the potential pocket of -11 K. $r_{\text{vdW}} = 5.08 a_0$, a_0 being the Bohr radius.

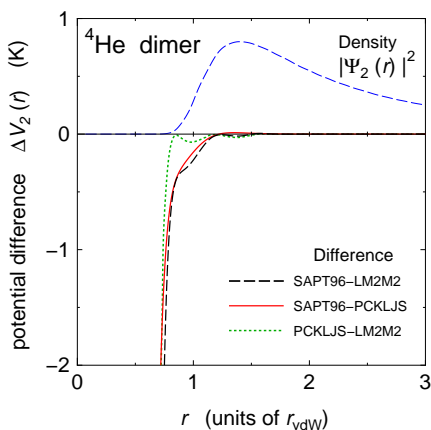


FIG. 2: (Color online) Difference in the realistic ${}^4\text{He}$ potentials $V_2(r)$ between the three example potentials. The dimer energy is $E_2 = -1.309$ mK(LM2M2), -1.615 mK(PCKLJS) and -1.744 mK(SAPT96). The repulsive core in the potentials is ≈ 1000 K at $r = 0.7 r_{\text{vdW}}$. The dashed blue curve is the same density of the dimer in Fig. 1 (in arbitrary unit).

tion in the fully nonadiabatic manner:

$$\left[T + \sum_{1=i<j}^A \lambda V_2(r_{ij}) - E_A \right] \Psi_A = 0, \quad (2.1)$$

where T is the kinetic energy and $V_2(r_{ij})$ is the realistic ${}^4\text{He}$ potential as a function of the pair separation r_{ij} (see below for the factor λ). Ψ_A has the total angular momentum $J = 0$. The mass parameter is fixed to $\frac{\hbar^2}{m} = 12.11928 \text{ K}\text{\AA}^2$ [49] where m is mass of ${}^4\text{He}$ atom.

The ${}^4\text{He}$ tetramer wave function Ψ_4 is calculated by expanding it in terms of the totally symmetrized L^2 -integrable K -type and H -type four-body Gaussian basis functions of the full 18 sets of the Jacobi coordinates as was explained

in paper I. The expansion coefficients and eigenenergy E_A are determined by diagonalizing the Hamiltonian in the large function space. The nonlinear parameters, such as the Gaussian ranges in geometric progressions, taken in the calculation were explicitly tabulated in paper I. Similar prescription is applied to the trimer (dimer) wave function $\Psi_3(\Psi_2)$.

For plotting the three-(four-)body Efimov spectrum of the ${}^4\text{He}$ trimer (tetramer), we calculate the energies of the ground and excited states, $E_3^{(0)}$ and $E_3^{(1)}$ ($E_4^{(0)}$ and $E_4^{(1)}$), as functions of the scattering length a of the two-body interaction. Following the literature [24, 50–52], we mimic the experimental tunability of the interatomic interactions via broad Feshbach resonances by directly altering the strength λ of the realistic ${}^4\text{He}$ potential in Eq. (2.1), which leads to the desired change of a (when $\lambda = 1$, the potential equals to the original one).

The realistic ${}^4\text{He}$ potentials have the same van der Waals potential $-C_6/r^6$ but the binding energy of the ${}^4\text{He}$ dimer ranges from 1.309 mK (LM2M2) to 1.744 mK (SAPT96) with some 30% difference (cf. Table I below) due to the variation in the short-range physics. We illustrate in Fig. 2 the potential differences between the three example potentials (LM2M2, PCKLJ and SAPT96). It is of interest to examine to what extent those differences affect the critical scattering lengths $a_-^{(v)}$ in the ${}^4\text{He}$ trimer and $a_-^{(4,v)}$ in the tetramer.

B. Three-(four-)body hyperradial potential

In order to investigate the short-range repulsive barrier in terms of the A -body hyperradius R_A ($A = 3, 4$), we derive the hyperradial wave function from our wave function $\Psi_A^{(v)}$. Although there are several conventions to define R_A , the present paper employs the definition in Refs. [53, 54] for the A -body system with an equal mass:

$$R_A = \left[\frac{2}{A} \sum_{j>i}^A (\mathbf{r}_i - \mathbf{r}_j)^2 \right]^{1/2}, \quad (2.2)$$

where \mathbf{r}_i is the position vector of particle i .

For the trimer, we have $R_3 = \sqrt{\frac{2}{3}(r_{12}^2 + r_{13}^2 + r_{23}^2)}$ which was taken in the calculations in Refs. [1, 26, 52], while Ref. [18] employed another definition of $R_3^{[18]} = \sqrt{\frac{1}{\sqrt{3}}(r_{12}^2 + r_{13}^2 + r_{23}^2)} \approx 0.93 R_3$.

We define the probability density of the A -body system, $\rho_A^{(v)}(R'_A)$ ($A = 3, 4$ and $v = 0, 1$), as a function of the hyperradius R'_A by

$$\rho_A^{(v)}(R'_A) = \langle \Psi_A^{(v)} | \frac{\delta(R_A - R'_A)}{R_A^{2D}} | \Psi_A^{(v)} \rangle, \quad (2.3)$$

where D is given by $D = (3N - 1)/2$ with $N = A - 1$ [53] and $\rho_A^{(v)}(R_A)$ is normalized as $\int_0^\infty \rho_A^{(v)}(R_A) R_A^{2D} dR = 1$ since $\langle \Psi_A^{(v)} | \Psi_A^{(v)} \rangle = 1$. In Appendix, we explain in more detail how we calculate Eq. (2.3) using $\Psi_A^{(v)}$ which is written in terms of the full sets of Jacobi coordinates.

We relate the hyperradial density $\rho_A^{(v)}(R_A)$ to the hyperradial wave function $f_A^{(v)}(R_A)$ ($v = 0, 1$) by

$$\rho_A^{(v)}(R_A) = \left| \frac{f_A^{(v)}(R_A)}{R_A^D} \right|^2, \quad (2.4)$$

and consider that $f_A^{(v)}(R_A)$ satisfies the single-channel hyperradial Schrödinger equation for the ^4He trimer and for the tetramer associated with the ground-state trimer:

$$\left[-\frac{\hbar^2}{m} \frac{d^2}{dR_A^2} + U_A(R_A) - E_A^{(v)} \right] f_A^{(v)}(R_A) = 0, \quad (2.5)$$

(cf. Eq. (4.4) in Ref. [53], Eq. (6) in Ref. [26] and Eq. (1) in Ref. [18]). In Eq. (2.5), the nonadiabatic effect and the coupling to other channels appearing in the hyperspherical framework are all renormalized into the A -body hyperradial potential $U_A(R_A)$ since $f_A^{(v)}(R_A)$ ($v = 0, 1$) is calculated from the fully nonadiabatic solution $\Psi_A^{(v)}$ and $E_A^{(v)}$ of the original Schrödinger equation (2.1).

We derive $U_A^{(v)}(R_A)$ ($v = 0, 1$) by

$$U_A^{(v)}(R_A) = \frac{\hbar^2}{m} \frac{d^2 f_A^{(v)}(R_A)}{dR_A^2} / f_A^{(v)}(R_A) - E_A^{(v)}. \quad (2.6)$$

The result should satisfy $U_A^{(0)}(R_A) = U_A^{(1)}(R_A)$ as the potential $U_A(R_A)$ in the Schrödinger Eq. (2.5); this will successfully be examined in Secs. III B and IV B.

At large R_3 , one would expect that $U_3(R_3)$ asymptotes to

$$U_3(R_3) \rightarrow -\frac{\hbar^2}{m} \frac{s_0^2 + \frac{1}{4}}{R_3^2} \quad (R_3 \gg r_{\text{vdW}}) \quad (2.7)$$

with $s_0 \approx 1.00624$ as the usual Efimov behavior of the potential [1, 18, 26]. It will be shown in Sec. III B that $U_3^{(v)}(R_3)$ ($v = 0, 1$) satisfy Eq. (2.7).

We note that if the two-body repulsive core at $r_{12} \approx r_{\text{vdW}}$ is the direct origin of the repulsive barrier in $U_A(R_A)$, the particles could come close together reaching $R_A \approx \sqrt{A-1} r_{\text{vdW}}$ when all the $r_{ij} \approx r_{\text{vdW}}$ in Eq. (2.2); but this will be denied in Secs. III B and IV B since the possible minimum R_A is derived as $R_A \approx (A-1) r_{\text{vdW}}$ ($A = 3, 4$) in the actual calculation.

III. RESULT FOR ^4He TRIMER

A. Three-body parameter

The calculated Efimov spectrum for the ^4He trimer is plotted in Fig. 3 with the solid curves; the trimer energies $E_3^{(0)}$ and $E_3^{(1)}$ are illustrated as functions of the scattering length a . Following the literature, we have drawn $(|E|/E_{\text{vdW}})^{1/4}$ versus $(|a|/r_{\text{vdW}})^{-1/2}$ so that both curves are graphically represented on the same scale. The scattering length a and the

energy E are scaled with $r_{\text{vdW}} (= 5.08 a_0$ [20]) and the van der Waals energy $E_{\text{vdW}} = \hbar^2/mr_{\text{vdW}}^2 (= 1.677$ K), respectively. The dashed curve shows the dimer energy. The vertical dotted line indicates the physical value $\lambda = 1$.

The result in Fig. 3 depends little on the seven kinds of the realistic potentials so that the curves are the same for different potentials within the thickness of the lines. We note that, in the case of the LM2M2 potential, almost the same figure as Fig. 3 was already reported by one of the authors (E.H.) and the collaborators [24] and by Gottobigio *et al.* [52].

In Fig. 3, $a_-^{(0)}$ and $a_-^{(1)}$ indicate the critical scattering lengths at which the trimer energies $E_3^{(0)}$ and $E_3^{(1)}$ intersect respectively the three-atom threshold on the $a < 0$ side. The calculated values of them are summarized in Table I together with the recent experimental values for the alkali-atom trimers [5–16] except for those on narrow Feshbach resonances. First of all, we emphasize that the seven realistic potentials give the same value as $a_-^{(0)}/a_0 = -48.2(1)$ and $a_-^{(1)}/a_0 = -832(1)$ showing a negligible contribution from the difference in their short-range details shown in Fig. 2.

Here, we introduce a modified van der Waals length, say \tilde{r}_{vdW} , for the scaled ^4He potential $\lambda V_2(r_{ij})$ that gives $a_-^{(0)}$ and $a_-^{(1)}$ with the λ values listed in Table I:

$$\tilde{r}_{\text{vdW}} = \frac{1}{2} (m\lambda C_6/\hbar^2)^{1/4} = \lambda^{1/4} r_{\text{vdW}}. \quad (3.1)$$

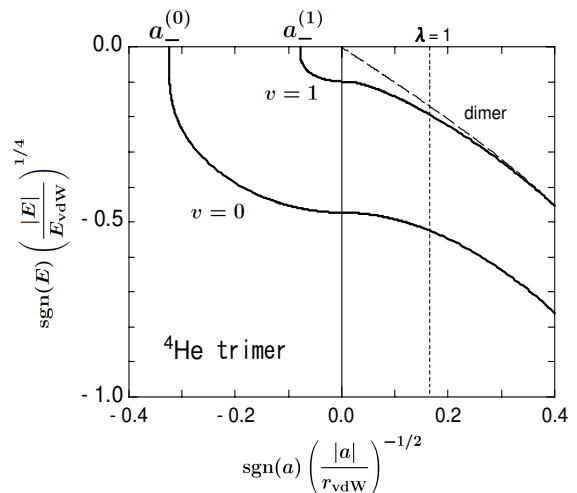


FIG. 3: Efimov spectrum for the ^4He trimer calculated with the seven realistic ^4He potentials, LM2M2, TTY, HFD-B, HFD-B3-FCII, SAPT96, CCSAPT07, and PCKLJS: trimer energy $E_3^{(v)}$ as a function of the scattering length a for the ground ($v = 0$) and excited ($v = 1$) states are shown as the solid curves, while the dimer energy is shown as the dotted curve. The curves for different potentials overlap with each other within the line thickness. To clarify the figure, a and E are scaled with the r_{vdW} and E_{vdW} , and raised to the power $-1/2$ and $1/4$, respectively. $a_-^{(0)}$ and $a_-^{(1)}$ denote respectively the scattering lengths where the trimer energies $E_3^{(0)}$ and $E_3^{(1)}$ intersect the three-atom threshold. The dotted line indicates the scattering length corresponding to the unscaled potential at $\lambda = 1$.

TABLE I: Scattering lengths for the first and second Efimov resonances, $a_-^{(0)}$ and $a_-^{(1)}$, where the Efimov spectra ($v = 0, 1$) cross the three-body threshold on the negative a side (cf. Fig. 3). They are calculated using the seven different realistic ${}^4\text{He}$ potentials (see text for λ and \tilde{r}_{vdW}). The values scaled with \tilde{r}_{vdW} are compared with experimental values scaled with r_{vdW} . Here, $r_{\text{vdW}}/a_0 = 5.08, 31.26, 32.49, 82.10$ and 101 for ${}^4\text{He}, {}^6\text{Li}, {}^7\text{Li}, {}^{85}\text{Rb}$ and ${}^{133}\text{Cs}$, respectively [20]. The potential names are arranged in the increasing order of the binding energy of the ${}^4\text{He}$ dimer, B_2 , at $\lambda = 1$.

${}^4\text{He}$ trimer		Ground state ($v = 0$)			Excited state ($v = 1$)		
Realistic potentials	B_2 (mK)	$a_-^{(0)}/a_0$	$a_-^{(0)}/\tilde{r}_{\text{vdW}}$	λ	$a_-^{(1)}/a_0$	$a_-^{(1)}/\tilde{r}_{\text{vdW}}$	λ
LM2M2	1.309	-48.26 ^a	-9.78	0.8901	-832 ^a	-165	0.9685
TTY	1.316	-48.29	-9.78	0.8902	-832	-165	0.9685
HFD-B3-FCI1	1.448	-48.22	-9.78	0.8891	-832	-165	0.9673
CCSAPT07	1.564	-48.21	-9.78	0.8881	-832	-165	0.9662
PCKLJS	1.615	-48.21	-9.78	0.8877	-832	-165	0.9658
HFD-B	1.692	-48.22	-9.78	0.8869	-832	-165	0.9651
SAPT96	1.744	-48.18	-9.77	0.8867	-831	-165	0.9647
Experiments		$a_-^{(0)}/a_0$	$a_-^{(0)}/r_{\text{vdW}}$		$a_-^{(1)}/a_0$	$a_-^{(1)}/r_{\text{vdW}}$	
Exp(${}^{133}\text{Cs}, {}^{85}\text{Rb}, {}^6, {}^7\text{Li}$)			$\approx -9.5 \pm 15\%$ ^b				
Exp (${}^{133}\text{Cs}$) [16]		-963(11)	-9.53(11)		-20190(1200)	-200(12)	
Exp (${}^6\text{Li}$) [9, 10]		-292	-9.34		-5752	-177	

^aRef. [52] gave $a_-^{(0)}/a_0 \sim -48.1$ and $a_-^{(1)}/a_0 \sim -975$ for LM2M2.

^bA value summarized in [12, 17–19] for experimental data [5–16].

The calculated and observed values of $a_-^{(0)}$ and $a_-^{(1)}$ are scaled by \tilde{r}_{vdW} for ${}^4\text{He}$ and by r_{vdW} for alkali atoms and are compared in Table I (the same applies to tetramers). For the ${}^4\text{He}$ trimer, $\lambda^{\frac{1}{4}} \approx 0.97$ for $a_-^{(0)}$ and ≈ 0.99 for $a_-^{(1)}$.

The calculated value of $a_-^{(0)}/\tilde{r}_{\text{vdW}} = 9.78(1)$ agrees with the universal value $a_-^{(0)}/r_{\text{vdW}} \approx -9.5 \pm 15\%$ obtained in the recent experiments and $a_-^{(0)}/r_{\text{vdW}} = -9.73(3) \pm 15\%$ calculated in Ref. [18], while $a_-^{(1)}/\tilde{r}_{\text{vdW}} = 165(1)$ for the excited state of the ${}^4\text{He}$ trimer [61] does not contradict the observed values $a_-^{(1)}/r_{\text{vdW}} = -177$ and $-200(12)$ for the second Efimov resonances in ${}^6\text{Li}$ and ${}^{133}\text{Cs}$, respectively.

The low-energy universal Efimov theory does not predict the absolute position of $a_-^{(0)}$, but predicts the ratio $a_-^{(1)}/a_-^{(0)}$ to have a universal value $a_-^{(1)}/a_-^{(0)} = 22.7$ [1, 3, 4]. According to the literature [23, 46, 55–57], effects of the finite interaction range and the van der Waals tail give corrections toward somewhat smaller values than 22.7; especially, a value of 17.1 was predicted in Ref. [23] in the limit of strongly entrance-channel-dominated Feshbach resonances. The experiments that measured both the $a_-^{(0)}$ and $a_-^{(1)}$ in the same atom gave the ratio $(a_-^{(1)}/a_-^{(0)})_{\text{exp}} = 21.0(1.3)$ and 19.7 for ${}^{133}\text{Cs}$ [16] and ${}^6\text{Li}$ [9, 10] respectively. In the present calculation of the ${}^4\text{He}$ trimer using the realistic ${}^4\text{He}$ potentials, we have also found that the ratio gets smaller than the universal value, giving $(a_-^{(1)}/a_-^{(0)})_{{}^4\text{He}} = 17.2$ [62].

B. Three-body repulsive barrier

Following the formulation of the hyperradial three-body potential in Sec. II B, we first calculate the wave function $\Psi_3^{(v)}$ in Eq. (2.1) using the LM2M2 potential, as an example (use of the other potentials give almost the same result), at the unitary limit ($|a| \rightarrow \infty$) given by $\lambda = 0.9743$. We obtain $E_3^{(0)} = -0.0501 E_{\text{vdW}}$ and $E_3^{(1)} = -9.36 \times 10^{-5} E_{\text{vdW}}$; the r.m.s. radius $\langle R_3^2 \rangle^{1/2}$ is $6.47 r_{\text{vdW}}$ ($v = 0$) and $94.2 r_{\text{vdW}}$ ($v = 1$). The ratio $E_3^{(0)}/E_3^{(1)} = 534$ is close to the ratio 531 in Ref. [23] in the case of a broad Feshbach resonance with the strength parameter $s_{\text{res}} = 100$. This again implies the applicability of the present calculation using the single-channel atom-atom potential to systems featuring broad Feshbach resonances.

Calculated three-body densities $|f_3^{(v)}(R_3)|^2$ are illustrated in Fig. 4 for $R_3 < 7 r_{\text{vdW}}$ and in Fig. 5 (log scale) for $R_3 < 25 r_{\text{vdW}}$ as the solid curve ($v = 0$) and the dotted red curve ($v = 1$). In Fig. 6, the three-body potentials $U_3^{(v)}(R_3)$ defined by Eq. (2.6) are shown as the solid curve ($v = 0$) and the dotted red curve ($v = 1$). Also shown, for the sake of reference, are the Efimov attraction, Eq. (2.7), in the dot-dash curve and the density $|f_3^{(0)}(R_3)|^2$ in the dashed blue curve (arbitrary unit).

A striking aspect of these figures is that the hyperradial potentials satisfy $U_3^{(0)}(R_3) = U_3^{(1)}(R_3)$ and converge to the Efimov attraction at large distances; this demonstrates the validity of the idea to construct the hyperradial Schrödinger equa-

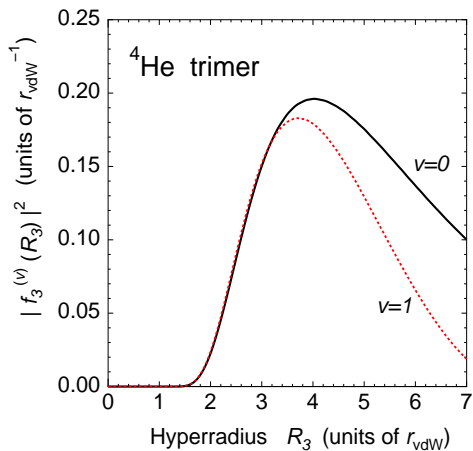


FIG. 4: (Color online) Probability density $|f_3^{(v)}(R_3)|^2$ ($v = 0, 1$) of the ${}^4\text{He}$ trimer ground (solid curve) and excited (dotted red curve) states versus the three-body hyperradius R_3 for $R_3 < 7 r_{\text{vdW}}$. The dotted curve has been multiplied by a factor 463 to emphasize that the two states exhibit the same shape of the strong short-range correlations for $R_3 \lesssim 3 r_{\text{vdW}}$.

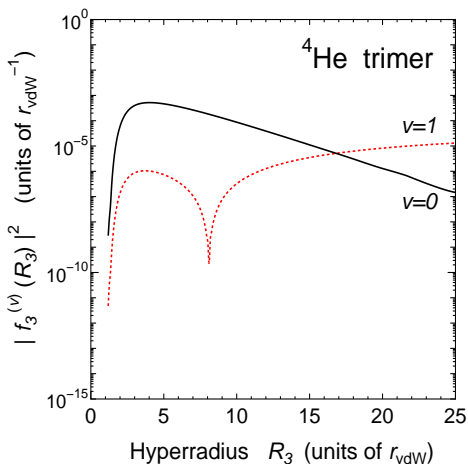


FIG. 5: (Color online) The same as Fig. 4 for $R_3 < 25 r_{\text{vdW}}$ in the log scale, but no factor is multiplied to the dotted curve.

tion (2.5) starting from the solution $\Psi_3^{(v)}$ and $E_3^{(v)}$ of the original Schrödinger equation (2.1).

From the behavior of the potentials $U_3^{(v)}(R_3)$ and the densities $|f_3^{(v)}(R_3)|^2$ ($v = 0, 1$), we recognize that there is a three-body repulsive barrier at $R_3 \approx 2 r_{\text{vdW}}$. Inside the barrier, $R_3 \lesssim 2 r_{\text{vdW}}$, the probability of finding the atoms is heavily suppressed. This result supports the finding, in Refs. [18, 26], of the appearance of the effective three-body repulsion with the adiabatic hyperspherical calculations. Our potential in Fig. 6 is close to the the hyperradial three-body potential for the first Efimov trimer state obtained in Fig. 3b of Ref. [18] and Figs. 1 and 7 of Ref. [26].

The hyperradius $R_3 \approx 2 r_{\text{vdW}}$ of the three-body repul-

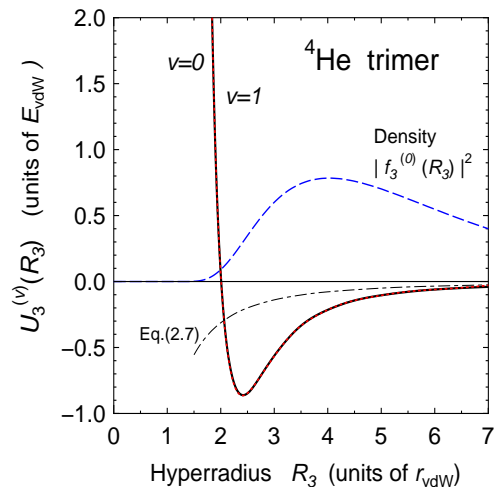


FIG. 6: (Color online) The three-body potential $U_3^{(v)}(R_3)$ ($v = 0, 1$) defined by Eq. (2.6) for the trimer ground (solid curve) and excited (dotted red curve) states. The two curves overlap with each other within the thickness of the lines. The dash-dotted curve shows the Efimov attraction, Eq. (2.7), and the dashed blue curve is for the density $|f_3^{(0)}(R_3)|^2$ in arbitrary unit.

sive barrier corresponds to the inter-particle distance $r_{ij} \approx \sqrt{2} r_{\text{vdW}}$ when all the r_{ij} are equal to each other in Eq. (2.2). The distance is $\sqrt{2}$ times larger than the radius of the two-body potential core $r_{12} \approx r_{\text{vdW}}$ and is located almost outside the region where the difference in the seven realistic potentials is seen in Fig. 2; this is due to the nonadiabatic three-body dynamics that, as was pointed out in Refs. [18, 26], the suppression of the two-body probability for $r_{ij} \lesssim r_{\text{vdW}}$ leads to the three-body repulsion for $R_3 \lesssim 2 r_{\text{vdW}}$.

IV. RESULT FOR ${}^4\text{He}$ TETRAMER

A. Four-body Efimov spectrum

Using the same method of papers I and II, we solved the four-body Schrödinger equation (2.1) for the ground ($v = 0$) and excited ($v = 1$) states of the ${}^4\text{He}$ tetramer changing the factor λ for the potentials. The four-body Efimov spectrum of $E_4^{(0)}$ and $E_4^{(1)}$ is plotted in Fig. 7 in the solid curves together with the spectrum of ${}^4\text{He}$ trimer in the thin solid blue curves.

We note that the four-body Efimov plot for the ${}^4\text{He}$ tetramer calculated with the *realistic* ${}^4\text{He}$ potential is reported for the first time in the present paper. Using effective two-body plus three-body Gaussian potentials, Gattobigio *et. al* [52] obtained a similar plot as Fig. 7 for the ${}^4\text{He}$ tetramer. We find two tetramer bound states, one deep and one shallow, tied to the trimer ground state; this agrees with the key prediction in Refs. [58, 59] that there are two universal four-body states associated with each Efimov trimer.

In Fig. 7, $a_-^{(4,0)}$ and $a_-^{(4,1)}$ denote the critical scattering lengths where the tetramer energies $E_4^{(0)}$ and $E_4^{(1)}$ cross the

TABLE II: The critical scattering lengths $a_-^{(4,0)}$ and $a_-^{(4,1)}$, where the tetramer energies $E_4^{(0)}$ and $E_4^{(1)}$ cross the four-body threshold on the negative a side (see Fig. 7). They are calculated with the seven different realistic ${}^4\text{He}$ potentials (see text for λ and \tilde{r}_{vdW}). The values scaled with \tilde{r}_{vdW} are compared with experimental values scaled with r_{vdW} . B_2 is the binding energy of the dimer at $\lambda = 1$.

${}^4\text{He}$ tetramer		Ground state ($v = 0$)			Excited state ($v = 1$)		
Realistic potentials	B_2 (mK)	$a_-^{(4,0)}/a_0$	$a_-^{(4,0)}/\tilde{r}_{\text{vdW}}$	λ	$a_-^{(4,1)}/a_0$	$a_-^{(4,1)}/\tilde{r}_{\text{vdW}}$	λ
LM2M2	1.309	-22.69	-4.69	0.8197	-43.98	-8.93	0.8832
TTY	1.316	-22.70	-4.69	0.8199	-43.96	-8.93	0.8832
HFD-B3-FCI1	1.448	-22.67	-4.69	0.8187	-43.95	-8.93	0.8821
CCSAPT07	1.564	-22.66	-4.69	0.8178	-43.95	-8.93	0.8812
PCKLJS	1.615	-22.66	-4.69	0.8174	-43.93	-8.93	0.8807
HFD-B	1.692	-22.67	-4.69	0.8166	-43.95	-8.93	0.8800
SAPT96	1.744	-22.65	-4.69	0.8165	-43.91	-8.92	0.8798
Experiments		$a_-^{(4,0)}/a_0$	$a_-^{(4,0)}/r_{\text{vdW}}$		$a_-^{(4,1)}/a_0$	$a_-^{(4,1)}/r_{\text{vdW}}$	
Exp (${}^{133}\text{Cs}$) [2]		-444(8)	-4.40(8)		-862(9)	-8.53(9)	
Exp (${}^{133}\text{Cs}$) [7]		-410	-4.06		-730	-7.23	
Exp (${}^{133}\text{Cs}$) [15]		-440(10)	-4.36(10)				
Exp (${}^7\text{Li}$) [14]		-94(4)	-2.9(1)		-236(10)	-7.26(31)	

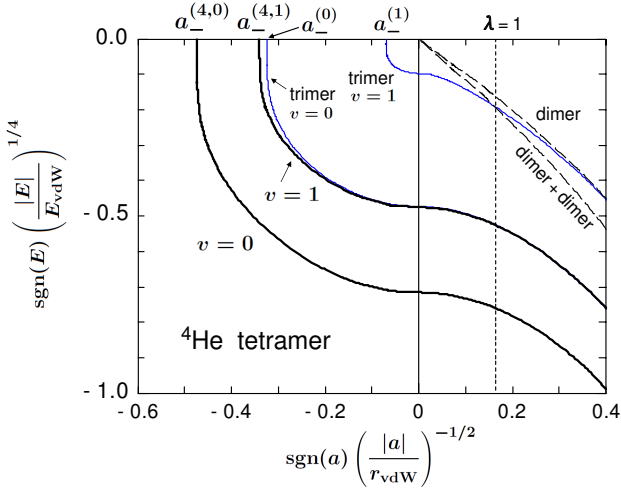


FIG. 7: (Color online) Efimov spectrum for the ${}^4\text{He}$ tetramer calculated with the seven realistic ${}^4\text{He}$ potentials, LM2M2, TTY, HFD-B, HFD-B3-FCI1, SAPT96, CCSAPT07, and PCKLJS: The scaled tetramer energy $E_4^{(v)}/E_{\text{vdW}}$ as a function of the scaled-inverse scattering length $(a/r_{\text{vdW}})^{-1}$ for the ground ($v = 0$) and excited ($v = 1$) states. The curves for different potentials overlap with each other within the line thickness. The thin solid blue curves denote the trimer spectrum which is the same as that in Fig. 3. $a_-^{(4,0)}$ and $a_-^{(4,1)}$ denote the critical scattering lengths where the tetramer energies $E_4^{(0)}$ and $E_4^{(1)}$ cross the four-atom threshold, respectively.

four-atom threshold. Their values are summarized in Table II for the realistic ${}^4\text{He}$ potentials together with the observed values for ${}^{133}\text{Cs}$ [2, 7, 15] and ${}^7\text{Li}$ [14]. Similarly to Table I

for the trimer, the seven realistic potentials give the same value as $a_-^{(4,0)}/a_0 = -22.7(1)$ and $a_-^{(4,1)}/a_0 = -44.0(1)$ showing that they are insensitive to the details of the potentials at short distances [63]. The calculated values of $a_-^{(4,0)}/\tilde{r}_{\text{vdW}} = -4.69(1)$ and $a_-^{(4,1)}/\tilde{r}_{\text{vdW}} = -8.93(1)$ do not contradict the corresponding observed values for the ${}^{133}\text{Cs}$ and ${}^7\text{Li}$ tetramers as seen in Table II.

Reference [59] predicted that the universal properties of the four-body system are directly related to the three-body subsystem as $a_-^{(4,0)} = 0.43 a_-^{(0)}$ and $a_-^{(4,1)} = 0.90 a_-^{(0)}$. The present calculation of the ${}^4\text{He}$ atoms using the realistic potentials gives consistent values of $a_-^{(4,0)} = 0.47 a_-^{(0)}$ and $a_-^{(4,1)} = 0.91 a_-^{(0)}$. The observed data for ${}^{133}\text{Cs}$ and ${}^7\text{Li}$ are in accordance with the prediction [59].

B. Four-body repulsive barrier

Using the nonadiabatic solution $\Psi_4^{(v)}$ ($v = 0, 1$) to the four-body Schrödinger equation (2.1), we calculate the probability density $|f_4^{(v)}(R_4)|^2$ and the potential $U_4^{(v)}(R_4)$, defined in Sec. II, as functions of the four-body hyperradius $R_4 = \sqrt{\frac{1}{2}(r_{12}^2 + r_{13}^2 + r_{14}^2 + r_{23}^2 + r_{24}^2 + r_{34}^2)}$. As for the ${}^4\text{He}$ realistic potential, we employ, the LM2M2 potential, as an example, at the unitary limit ($|a| \rightarrow \infty$) with $\lambda = 0.9743$; we have $E_4^{(0)} = -0.262 E_{\text{vdW}}$ and $E_4^{(1)} = -0.0510 E_{\text{vdW}}$. The r.m.s. hyperradius $\langle R_4^2 \rangle^{1/2}$ is $5.95 r_{\text{vdW}}$ ($v = 0$) and $38.0 r_{\text{vdW}}$ ($v = 1$).

The density distributions $|f_4^{(v)}(R_4)|^2$ are illustrated in Fig. 8 for $R_4 < 10 r_{\text{vdW}}$ and in Fig. 9 (log scale) for

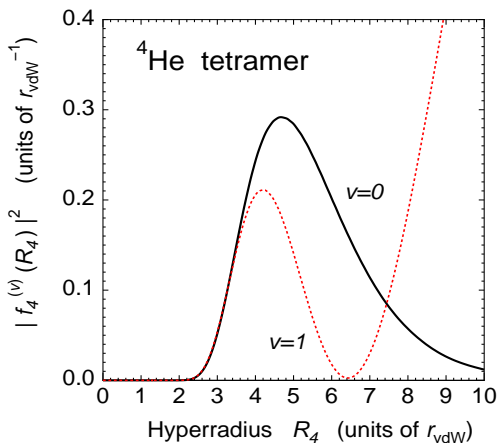


FIG. 8: (Color online) Probability density $|f_4^{(v)}(R_4)|^2$ ($v = 0, 1$) of the ${}^4\text{He}$ tetramer ground (solid curve) and excited (dotted red curve) states as a function of the hyperradius R_4 for $R_4 < 10 r_{\text{vdW}}$. The density is normalized as $\int_0^\infty |f_4^{(v)}(R_4)|^2 dR_4 = 1$. The dotted curve has been multiplied by a factor 25 to emphasize that the two tetramer states exhibit the same shape of the strong short-range correlations for $R_4 \lesssim 3.5 r_{\text{vdW}}$.

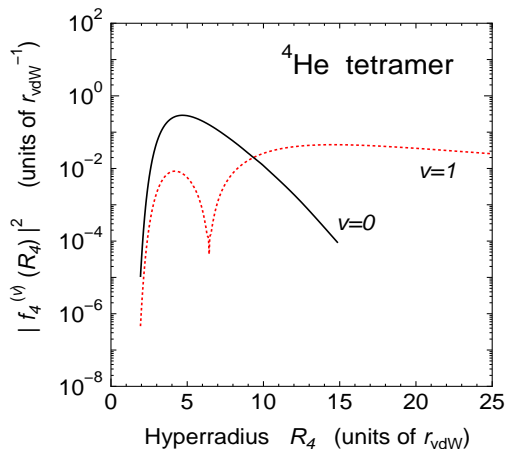


FIG. 9: (Color online) The same as Fig. 8 for $R_4 < 25 r_{\text{vdW}}$ in the log scale, but no factor is multiplied to the dotted curve.

$R_4 < 25 r_{\text{vdW}}$ by the solid curve ($v = 0$) and the dotted red curve ($v = 1$). The four-body potentials $U_4^{(v)}(R_4)$ are shown in Fig. 10 as the solid curve ($v = 0$) and the dotted red curve ($v = 1$) [64]. We find that the condition $U_4^{(0)}(R_4) = U_4^{(1)}(R_4)$ is satisfied, which is required as the potential of the Schrödinger equation (2.5) for the tetramer states attached to the trimer ground state; the two states are to be generated by the same hyperradial potential dominantly for the relative motion between the trimer ground state and the fourth atom, for instance, as seen in Fig. 2 of Ref. [59].

From the behavior of the potentials $U_4^{(v)}(R_4)$ and the density distributions $|f_4^{(v)}(R_4)|^2$ ($v = 0, 1$), we recognize a strong repulsive barrier at $R_4 \approx 3 r_{\text{vdW}}$ that heavily sup-

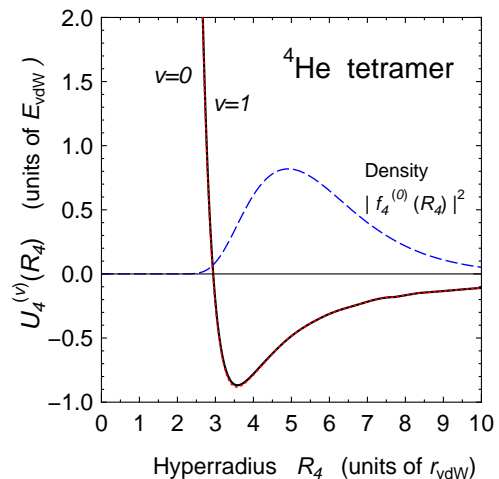


FIG. 10: (Color online) The four-body potential $U_4^{(v)}(R_4)$ ($v = 0, 1$) defined by Eq. (2.6) for the ${}^4\text{He}$ tetramer ground (solid curve) and excited (dotted red curve) states. The two curves overlap with each other within the thickness of the lines. The dashed blue curve is for the density $|f_4^{(0)}(R_4)|^2$ in arbitrary unit.

presses the four-body density in the region $R_4 \lesssim 3 r_{\text{vdW}}$, which makes $a_{-}^{(4,0)}$ and $a_{-}^{(4,1)}$ insensitive to the short-range details of the interactions seen in Fig. 2. The four-body repulsion radius $R_4 \approx 3 r_{\text{vdW}}$ corresponds to the interparticle distance $r_{ij} \approx \sqrt{3} r_{\text{vdW}}$ when all the r_{ij} are equal to each other in Eq. (2.2). The distance is $\sqrt{3}$ times larger than the two-body core radius $r_{12} \approx r_{\text{vdW}}$ and is located outside the region where the short-range details of the seven realistic potentials differ from each other (Fig. 2). Inversely, if all the r_{ij} are artificially replaced by the two-body core radius, the four-body repulsion radius becomes $R_4 \approx \sqrt{3} r_{\text{vdW}}$. The increase of the core radius R_4 by factor $\sqrt{3}$ in the actual four-body system is due to the nonadiabatic four-body dynamics which is an extension of the mechanism discovered in Ref. [18] for the three-body systems.

For four-body bound states, the universal repulsion appears at larger distance than the three-body ones, suggesting that the four-body states tend to be more universal than the three-body ones. We note that in Ref. [60] for the study of N -body ${}^4\text{He}$ clusters ($N = 3 - 10$) with the LM2M2 potential, effective N -body hyperradial potentials were approximately calculated on the basis of the Monte Carlo methods combined with the adiabatic hyperspherical approach and were used to calculate the N -body excited bound states. The radius of the repulsive potential core becomes larger with increasing N ; the radius in the potential figure seems consistent with the present result within $\sim 10\%$ for $N = 3$ and 4. It is then conjectured that the universal N -body repulsion would generally appear in the Efimov associated N -body bound states ($N > 3$), rendering those states universal and insensitive to short-range details.

V. SUMMARY

We have investigated the universality in the ^4He trimer and tetramer using the seven realistic ^4He potentials and presented that even ^4He potentials are consistent with measurements of broad Feshbach resonances in ultracold atoms, which shows the large extent of universality in three- and four-body systems with interactions featuring van der Waals tails.

We calculated the critical scattering lengths $a_-^{(v)}$ ($a_-^{(4,v)}$) ($v = 0, 1$) at which the trimer (tetramer) energies cross the three-(four-)atom threshold. From the nonadiabatic total wave function $\Psi_A^{(v)}$ ($A = 3, 4$) that is described in terms of the full sets of the Jacobi coordinates, we derived the hyperradial wave function $f_A^{(v)}(R_A)$ and potential $U_A^{(v)}(R_A)$ as a function of the A -body hyperradius R_A . The main conclusions are summarized as follows:

(i) We found the following universality in the ^4He tetramer: The four-body hyperradial potentials $U_4^{(v)}(R_4)$ ($v = 0, 1$) have a repulsive barrier at the four-body hyperradius $R_4 \approx 3 r_{\text{vdW}}$, which corresponds to the pair distance $r_{ij} \approx \sqrt{3} r_{\text{vdW}}$ when all the r_{ij} are equal to each other. This pair distance is significantly larger than the radius $r_{12} \approx r_{\text{vdW}}$ of the two-body repulsive core in the realistic ^4He potentials. Inside the barrier, $R_4 \lesssim 3 r_{\text{vdW}}$, the probability density $|f_4^{(v)}(R_4)|^2$ to find the atoms is heavily suppressed. The four-body barrier prevents the particles from getting close together to explore non-universal features of the interactions at short distances; hence, the critical scattering lengths are not affected by the difference in the short-range details of the interactions. The seven realistic ^4He potentials give the same value as $a_-^{(4,0)}/\tilde{r}_{\text{vdW}} = -4.69(1)$ and $a_-^{(4,1)}/\tilde{r}_{\text{vdW}} = -8.93(1)$, which do not contradict the corresponding values obtained in the experiments in ultracold gases of the alkali-metal atoms.

(ii) As for the universality in the ^4He trimer, we obtained the following result, which is consistent with that has been reported in Refs. [18, 26]: The three-body hyperradial potentials $U_3^{(v)}(R_3)$ ($v = 0, 1$) have a repulsive barrier at $R_3 \approx 2 r_{\text{vdW}}$, inside which the probability density $|f_3^{(v)}(R_3)|^2$ of finding the atoms is heavily suppressed. The hyperradius of the barrier corresponds to the pair distance $r_{ij} \approx \sqrt{2} r_{\text{vdW}}$ when all the r_{ij} are equal to each other. The seven realistic ^4He potentials give the same value of the universal three-body parameters as $a_-^{(0)}/\tilde{r}_{\text{vdW}} = -9.78(1)$ and $a_-^{(1)}/\tilde{r}_{\text{vdW}} = -165(1)$ independently of the short-range details of the potentials and

are consistent with the corresponding values obtained in the ultracold-atom experiments.

(iii) It will be one of the future subjects whether the four-body repulsive barrier at hyperradius $R_4 \approx 3 r_{\text{vdW}}$ also appears for deeper pairwise interactions that supports many two-body bound states like alkali atoms.

Appendix

We explain how to calculate $\rho_3(R)$ of Eq. (2.3) (the suffix 3 of R_3 is omitted). It is difficult to perform the integration (2.3) with the hyperradius R treated explicitly since Ψ_3 is not given as a function of R . We expand $\rho_3(R)$ in terms of Gaussians

$$\rho_3(R) = \sum_{n=1}^{n_{\text{max}}} c_n e^{-\nu_n R^2} \quad (5.1)$$

taking the range parameters $\{\nu_n\}$ in a geometric progression (e.g. Eqs. (2.10)–(2.13) in paper I). The coefficients c_n are obtained by solving a set of linear equations

$$\sum_{n=1}^{n_{\text{max}}} A_{in} c_n = B_i \quad (i = 1, \dots, n_{\text{max}}) \quad (5.2)$$

with the matrix elements

$$\begin{aligned} A_{in} &= \int_0^\infty e^{-(\nu_i + \nu_n)R^2} R^5 dR = (\nu_i + \nu_n)^{-3}, \\ B_i &= \int_0^\infty \rho_3(R') e^{-\nu_i R'^2} R'^5 dR' = \langle \Psi_3 | e^{-\nu_i R^2} | \Psi_3 \rangle \\ &= \langle \Psi_3 | e^{-\frac{2}{3}\nu_i(r_{12}^2 + r_{23}^2 + r_{31}^2)} | \Psi_3 \rangle. \end{aligned} \quad (5.3)$$

B_i is nothing but the expectation value of a three-body force of Gaussian shape, which is easily calculated. We took the set of Gaussian ranges in a geometric progression $\{n_{\text{max}} = 60, R_1 = 0.2 r_{\text{vdW}}, R_{n_{\text{max}}} = 80 r_{\text{vdW}}\}$ where $\nu_n = 1/R_n^2$. This method also applies to the ^4He tetramer.

Acknowledgement

The authors would like to thank Dr. S. Endo for valuable discussions and careful reading the manuscript. The numerical calculations were performed on HITACHI SR16000 at KEK and at YIFP in Kyoto University.

[1] V. Efimov, *Yad. Fiz.* **12**, 1080 (1970) [*Sov. J. Nucl. Phys.* **12**, 589 (1971)]; *Nucl. Phys. A* **210**, 157 (1973).
 [2] F. Ferlaino, A. Zenesini, M. Berninger, B. Huang, H.-C. Nägerl, and R. Grimm, *Few-Body Syst.* **51**, 113 (2011)
 [3] E. Braaten and H-W. Hammer, *Phys. Reports*, **428**, 259 (2006).
 [4] E. Braaten and H-W. Hammer, *Annals of Physics* **322**, 120 (2007).

[5] T. Kraemer, M. Mark, P. Waldburger, J.G. Danzl, C. Chin, B. Engeser, A.D. Lange, K. Pilch, A. Jaakkola, H.-C. Nägerl, R. Grimm, *Nature* **440**, 315 (2006).
 [6] S.E. Pollack, D. Dries, and R.G. Hulet, *Science* **326**, 1683 (2009).
 [7] F. Ferlaino, S. Knoop, M. Berninger, W. Harm, J.P. D'Incao, H.-C. Nägerl, and R. Grimm, *Phys. Rev. Lett.* **102**, 140401 (2009).

- [8] N. Gross, Z. Shotan, S. Kokkelmans, and L. Khaykovich, Phys. Rev. Lett. **103**, 163202 (2009).
- [9] A.N. Wenz, T. Lompe, T.B. Ottenstein, F. Serwane, G. Zürn, and S. Jochim, Phys. Rev. A **80**, 040702(R) (2009).
- [10] J.R. Williams, E.L. Hazlett, J.H. Huckans, R.W. Stites, Y. Zhang, and K.M. O'Hara, Phys. Rev. Lett. **103**, 130404 (2009).
- [11] N. Gross, Z. Shotan, S. Kokkelmans, and L. Khaykovich, Phys. Rev. Lett. **105**, 103203 (2010).
- [12] M. Berninger, A. Zenesini, B. Huang, W. Harm, H.-C. Nägerl, F. Ferlaino, R. Grimm, P. S. Julienne, and J.M. Hutson, Phys. Rev. Lett. **107**, 120401 (2011).
- [13] R.J. Wild, P. Makotyn, J.M. Pino, E.A. Cornell, and D.S. Jin, Phys. Rev. Lett. **108**, 145305 (2012).
- [14] P. Dyke, S.E. Pollack, and R.G. Hulet, Phys. Rev. A **88**, 023625 (2013).
- [15] A. Zenesini, B. Huang, M. Berninger, S. Besler, H.-C. Nägerl, F. Ferlaino, R. Grimm, C. H. Greene, and J. von Stecher, New J. Phys. **15**, 043040 (2013).
- [16] B. Huang, L.A. Sidorenkov, R. Grimm, and J.M. Hutson, Phys. Rev. Lett. **112**, 190401 (2014).
- [17] O. Machtey, Z. Shotan, N. Gross, and L. Khaykovich, Phys. Rev. Lett. **108**, 210406 (2012).
- [18] J. Wang, J.P. D'Incao, B.D. Esry, and C.H. Greene, Phys. Rev. Lett. **108**, 263001 (2012).
- [19] S. Roy, M. Landini, A. Trenkwalder, G. Semeghini, G. Spagnolli, A. Simoni, M. Fattori, M. Inguscio, and G. Modugno, Phys. Rev. Lett. **111**, 053202 (2013).
- [20] C. Chin, R. Grimm, P. Julienne, and E. Tiesinga, Rev. Mod. Phys. **82**, 1225 (2010).
- [21] C. Chin, arXiv:1111.1484.
- [22] P. K. Sørensen, D. V. Fedorov, A.S. Jensen, and N. T. Zinner, Phys. Rev. A **86**, 052516 (2012).
- [23] R. Schmidt, S.P. Rath, and W. Zwerger, Eur. Phys. J. B **85**, 386 (2012).
- [24] P. Naidon, E. Hiyama and M. Ueda, Phys. Rev. A **86**, 012502 (2012).
- [25] M.R. Hadizadeh, M.T. Yamashita, L. Tomio, A. Delfino, T. Frederico, Phys. Rev. A **87**, 013602 (2013).
- [26] P. Naidon, S. Endo and M. Ueda, Phys. Rev. A **90**, 022106 (2014).
- [27] P. Naidon, S. Endo and M. Ueda, Phys. Rev. Lett. **112**, 105301 (2014).
- [28] M. Kamimura, Phys. Rev. A **38**, 621 (1988).
- [29] H. Kameyama, M. Kamimura and Y. Fukushima, Phys. Rev. C **40**, 974 (1989).
- [30] E. Hiyama, Y. Kino and M. Kamimura, Prog. Part. Nucl. Phys. **51**, 223 (2003).
- [31] E. Hiyama, Few-Body Systems **53**, 189 (2012).
- [32] E. Hiyama, Prog. Theor. Exp. Phys. **2012**, 01A204 (2012).
- [33] E. Hiyama and M. Kamimura, Phys. Rev. A **85**, 022502 (2012).
- [34] E. Hiyama and M. Kamimura, Phys. Rev. A **85**, 062505 (2012).
- [35] R.A. Aziz and M.J. Slaman, J. Chem. Phys. **94**, 8047 (1991).
- [36] K.T. Tang, J.P. Toennies and C.L. Yiu, Phys. Rev. Lett. **74**, 1546 (1995).
- [37] R.A. Aziz, F.R.W. McCourt and C.C.K. Wong, Mol. Chem. Phys. **61**, 1487 (1987).
- [38] T. van Mourik and J. H. van Lenthe, J. Chem. Phys. **102**, 7479 (1995).
- [39] R. A. Aziz, A. R. Janzen, and M. R. Moldover, Phys. Rev. Lett. **74**, 1586 (1995).
- [40] A.R. Jansen and R.A. Aziz, J. Chem. Phys. **107**, 914 (1997).
- [41] H. L. Williams, T. Korona, R. Bukowski, B. Jeziorski, and K. Szalewicz, Chem. Phys. Lett. **262**, 431 (1996).
- [42] T. Korona, H. L. Williams, R. Bukowski, B. Jeziorski, and K. Szalewicz, J. Chem. Phys. **106**, 5109 (1997).
- [43] M. Jeziorska, W. Cencek, K. Patkowski, B. Jeziorski, and K. Szalewicz, J. Chem. Phys. **127**, 124303 (2007).
- [44] M. Przybytek, W. Cencek, J. Komasa, G. Lach, B. Jeziorski and K. Szalewicz, Phys. Rev. Lett. **104**, 183003 (2010); Phys. Rev. Lett. **108**, 129902(E) (2012) [Erratum].
- [45] W. Cencek, M. Przybytek, J.B. Mehl, J. Komasa, B. Jeziorski and K. Szalewicz, J. Chem. Phys. **136**, 224303 (2012).
- [46] Y. Wang and P.S. Julienne, Nature Physics **10**, 768 (2014).
- [47] R.E. Grisenti, W. Schollkopf, J.P. Toennies, G.C. Hegerfeldt, T. Kohler, and M. Stoll, Phys. Rev. Lett. **85**, 2284 (2000).
- [48] R. Brühl, A. Kalinin, O. Kornilov, J.P. Toennis, G.C. Herelfeld and M. Stoll, Phys. Rev. Lett. **95**, 06002 (2005).
- [49] V. Roudnev and M. Cavagnero, J. Phys. B: At. Mol. Opt. Phys. **45**, 025101 (2012).
- [50] B.D. Esry, C.D. Lin, and C.H. Greene, Phys. Rev. A **54**, 394 (1996).
- [51] P. Barletta and A. Kievsky, Phys. Rev. A **64**, 042514 (2001).
- [52] M. Gattobigio, A. Kievsky, and M. Viviani, Phys. Rev. A **86**, 042513 (2012).
- [53] M. Fabre de la Ripplé, Ann. Phys.(N.Y.) **147**, 281 (1983).
- [54] M. Gattobigio, A. Kievsky, M. Viviani, and P. Barletta, Phys. Rev. A **79**, 032513 (2009).
- [55] J.P. D'Incao, C. H. Greene, and B. D. Esry, J. Phys. B **42**, 044016 (2009).
- [56] L. Platter, C. Ji, and D.R. Phillips, Phys. Rev. A **79**, 022702 (2009).
- [57] M. Thøgersen, D.V. Fedorov, and A.S. Jensen, Phys. Rev. A **78**, 020501(R) (2008).
- [58] H.-W. Hammer and L. Platter, Eur. Phys. J. A **32**, 113 (2007).
- [59] J. von Stecher, J.P. D'Incao and C.H. Greene, Nature Phys., **5**, 417 (2009).
- [60] D. Blume and C.H. Greene, J. Chem. Phys. **112**, 8053 (2000).
- [61] It is hard to calculate precisely $a_-^{(1)}$ of the excited trimer state that has an extremely large size at $E_3^{(1)} \approx 0$. We took the maximum range of the Gaussians to be $4,000 r_{\text{vdW}}$ with an increased number of basis when calculating $a_-^{(v)}$ ($a_-^{(4,v)}$). We note that, if a smaller-size (worse) three-body basis set is *artificially* employed, the solid curve ($v = 1$) in Fig. 3 shifts slightly to the right (namely, the eigenstate becomes shallower), which gives a larger value of $|a_-^{(1)}|/\tilde{r}_{\text{vdW}}$, even *closer* to the corresponding observed data for the alkali atoms.
- [62] The same as the comments on $|a_-^{(1)}|/r_{\text{vdW}}$ in [61] for the ratio $a_-^{(1)}/a_-^{(0)}$.
- [63] Using effective two-body plus three-body Gaussian potentials without the van der Waals tail, Ref. [52] gave $a_-^{(4,0)}/a_0 = -19.6$ and $a_-^{(4,1)}/a_0 = -39.8$, respectively. Their absolute values are by some 10 – 15% smaller than those in the present work probably due to the lack of the long-range tail; the same tendency is seen in the trimer.
- [64] Since the dotted curve becomes singular in the vicinity of $R_4 = 6.4 r_{\text{vdW}}$ where $f_4^{(1)}(R_4) = 0$ in Eq. (2.6), we connected smoothly the lines on the both sides of the vicinity. When the Schrödinger equation (2.5) is solved using this smoothed potential, the condition that the excited-state wave function should have a node at $R_4 = 6.4 r_{\text{vdW}}$ is guaranteed by the orthogonality to the ground-state wave function. This situation is the same for the case of the trimer excited state whose wave function $f_3^{(1)}(R_3)$ has a node at $R_3 = 8.1 r_{\text{vdW}}$ (Fig. 5).